


## Investigation of the high-spin yrast band structure of $^{236-246}\text{Pu}$ isotopes

Ashwaq F. Jaafer and Falih H. Al-Khudair 

*Department of Physics, College of Education for Pure Sciences, University of Basrah, Basrah, Iraq*



(Received 10 June 2022; accepted 10 November 2022; published 9 December 2022)

The available data on some actinide nuclei point to certain significant features of the rotational yrast band and other excited bands. The rotational properties of plutonium isotopes ( $^{236-346}\text{Pu}$ ) were studied via projected shell model (PSM). Calculations are based on the Hamiltonian of the PSM which includes the formed part of a single particle, the  $Q-Q$  force, and the residual interaction of monopole and quadrupole pairings. The results of the calculated energy levels of the yrast band are then compared with available experimental data and a good agreement has been found. The crossing between two-quasiparticle (2qp) excited bands and the ground state band (g band) in the high-spin regions has been analyzed in terms of band diagrams. The upbendings observed in the kinematic moments of inertia ( $j^{(1)}$  MOI) curves for  $^{236-346}\text{Pu}$  isotopes are due to the effect of two aligning nucleons that occupy excited bands and the  $\nu(j_{15/2})$ ,  $\pi(i_{13/2})$  high- $j$  intruder orbits. The PSM successfully reproduces the observed upbending in  $j^{(1)}$  as well as the upturning and downturning in  $j^{(2)}$ . For the  $^{240}\text{Pu}$  isotope, the PSM predicts a simultaneous alignment of neutrons  $\nu^2 [1/2, -7/2] K^\pi = 4^+$  and protons  $\pi^2 [-3/2, 5/2] K^\pi = 1^+$  bands cross the g band at spin  $I = 22$ . We expect it to be mainly responsible for the disagreement at  $I = 22$ . Furthermore, electric quadrupole transition probabilities  $B(E2)$  and the gyromagnetic factor ( $g$  factor) for the yrast band energy levels are also studied.

DOI: [10.1103/PhysRevC.106.064309](https://doi.org/10.1103/PhysRevC.106.064309)

### I. INTRODUCTION

The problem of heavy nuclei with a prohibitively complex system can be solved by simple realistic approaches that rely on pairing effects [1]. The Bardeen-Cooper-Schrieffer (BCS) theory can be seen as a microscopic model that deals with strong pairing correlations between the nucleons [2]. From another point of view, the pairing phenomenon describes accurately the collective properties of deformed valence shell(s) in an even-even nucleus. For an efficient quantitative description via the complete BCS approach, the issue of the strong interaction can be simplified by using a quasiparticle rather than particle system. However, extending the superconductivity theory requires taking into account the effect of correlated pairs and implementing Hartree-Fock-Bogoliubov (HFB) equations [3]. A general solution of the deformed HFB equations provides quasiparticle operators  $a_i^\dagger, a_i$  with its vacuum  $|0\rangle$  and the number of single-particle orbits,  $i$ . The study of the quasiparticle excitations may support our findings on several high-spin phenomena [4,5]. Many quasiparticle alignments with their angular momenta provide us with a basic understanding of the single-particle excitations of the nuclear system under extraordinary new conditions. It is a new symmetrical breaking within the deformed basis of a multiquasiparticle system [6].

The ground state band of deformed nuclei has many rotational properties. One of these properties is known as the moment of inertia (MOI). The variety in MOI at both high and low spins can be interpreted in relation to the changes in pairing correlations between the nucleons of  $i_{13/2}$  and  $h_{11/2}$

orbits in rare-earth nuclei. The Coriolis forces have very noticeable effects on pairing correlations between neutrons  $j_{15/2}$  and protons  $i_{13/2}$  at high angular momentum of the rotating actinide nuclei [7,8]. To investigate the high-spin states of actinide nuclei, the targets of enriched  $^{240}\text{Pu}$  and  $^{248}\text{Cm}$  are bombarded with beams of  $^{208}\text{Po}$  [9]. The microscopic calculations predict that the proton alignment of the  $i_{13/2}$  intruder orbit is responsible for the strong presence of backbending in the  $^{244,246}\text{Pu}$ , but the irregularity is less pronounced in the neighboring  $^{242}\text{Pu}$  [10].

The projected shell model (PSM) is an improved tool to describe the deformed nuclei [11–14]. The procedure of the PSM calculations is based on the Nilsson model which adjusts the observed rotational bands to fill the shell of the proper individual nucleus. A few quasiparticles that occupy the orbits close to the Fermi level are selected to construct the projected deformed basis. Pairing correlations between nucleons are incorporated into the deformed basis by using the BCS treatment. Sheikh *et al.* [15–19] have proposed an extension of PSM, introducing a three-dimensional angular momentum projection, made of a triaxial Nilsson plus a BCS deformed intrinsic wave function for the purpose of improving the description of rotational and transitional nuclei.

Extending the PSM to Heavy Shell Model (HSM) provides an opportunity to describe the collective excitations relevant to deformed actinide nuclei ( $^{240}\text{Pu}$ ,  $^{232,234}\text{U}$ ,  $^{230,232}\text{Th}$ ). However, the  $D$ -pairs excitations ( $D_0(K^\pi = 2^+)$ ,  $D_2(K^\pi = 2^+)$ ) have been added to the intrinsic basis of the PSM [20]. The progressive increase of  $J^{(1)}$  and  $J^{(2)}$  in even and odd protons when  $N = 114$  isotones is due to the processes of

proton alignment in the high intruding orbit [21]. Moreover, the behavior of  $j^{(1)}$  in some even-even transuranium nuclei ( $^{246-252}\text{Cf}$ ,  $^{250-256}\text{Fm}$ ,  $^{252-258}\text{No}$ ) are the same along the yrast line. The upbending (upturning and downturning) in  $J^{(1)}$  ( $J^{(2)}$ ) at high-spin regions caused by band crossing is attributed to aligning pairs of  $i_{13/2}$  protons [22]. The investigations of rotational properties of  $^{256-260}\text{Rf}$  nuclei show that the  $j^{(1)}$  of the three Rf isotopes increased gently when the spin is  $I \leq 16$ , and then rises immediately in the next region. Eventually, the aligning nucleon pairs then lead to a structure change in the yrast bands [23]. The  $^{236-246}\text{Pu}$  isotopes exhibit a striking behavior in their respective yrast band which varies from one nucleus to another [24,25]. Thus, they become an efficient tool in the study of the rotational properties of deformed nuclei. The aims of the present work are as follows:

- (1) Carry out systematic PSM calculations so as to investigate the structure of yrast bands in  $^{236-246}\text{Pu}$  isotopes.
- (2) Uncover the influence of two-quasiparticle (2qp) excitation energy bands on the structure of the yrast band in addition to investigating the multiquasiparticle occupancy of specific orbitals.
- (3) Identify the effect that the proximity of orbits at the Fermi level has on the structure of energy bands.
- (4) Analyze the systematic changes in MOI according to the alignment of the pairs of quasiparticles which occupy the intruding orbits in the vicinity of the Fermi level, and discuss the possible reasons for the appearance of upbending and backbending in the MOI curves.

The paper includes four sections. The basic concepts of the PSM are explained in Sec. II. In Sec. III the rotational properties of the yrast band levels, which include kinematic and dynamic moments of inertia, are discussed by performing the PSM calculations; then at the end of this section, the  $B(E2)$  and  $g$ -factor calculations are performed. Finally, a conclusion is drawn in Sec. IV.

## II. THE THEORY OF PROJECTED SHELL MODEL

The intrinsic deformed basis of the Nilsson model plays a major role in the compilation of PSM calculations. In heavy nuclei, the specified valence space of the PSM is  $N = 4, 5, 6$  for the proton and  $N = 5, 6, 7$  for the neutron [26,27]. The exact solution of Nilsson + BCS provides multiquasiparticles in different single-particle orbits. The truncation of the basis is an essential tool in PSM applied to a large number of quasiparticle levels around the Fermi surface [11]. The truncated space is defined by the set of quasiparticle (qp) states  $|\phi_k\rangle$ . In the deformation system, the remaining problem is the breaking of the rotational symmetry [28,29], which is violated by the generalization of a mean-field theory (BCS + HFB) (but the axial symmetry is conserved). To restore rotational symmetries, the transformation of the intrinsic function  $|\phi\rangle$  to a system of body-fixed  $|\psi\rangle$  is done via the intricate angular momentum projection method [30–32]. The trail wave function of PSM is demonstrated as a linear combination of the Slater determinants, constructed from quasiparticle vacuums which have a good angular momentum projection. The fol-

lowing interesting wave function is given in Ref. [11]:

$$|\psi_M^I\rangle = \sum_k f_k^I \hat{P}_{MK}^I |\phi_k\rangle, \quad (1)$$

where  $\hat{P}_{MK}^I$  is the projection operator on the multiquasiparticle states.  $M$  is the projection of the total angular momentum  $I$ .  $f_k$  represents the weights of the basis states determined by making the Hamiltonian shell model diagonal. For even-even nuclei, we can consider the following multiquasiparticle configurations:

$$|\phi_k\rangle = |0\rangle, a_{v_i}^\dagger a_{v_j}^\dagger |0\rangle, a_{\pi_i}^\dagger a_{\pi_j}^\dagger |0\rangle, a_{v_i}^\dagger a_{v_j}^\dagger a_{\pi_i}^\dagger a_{\pi_j}^\dagger |0\rangle, \quad (2)$$

where  $a^\dagger$  is the quasiparticle creation operator, while  $v_i$  and  $v_j$  ( $\pi_i$  and  $\pi_j$ ) refer to the Nilsson quantum numbers for  $\nu(h_{11/2}, i_{13/2}, j_{15/2})$  [ $\pi(g_{9/2}, h_{11/2}, i_{13/2})$ ] orbits which are labeled in each deformed single-particle state in the Nilsson diagram.  $|0\rangle$  is the BCS ground state. The eigenvalue equations for each  $I$  are written as

$$\begin{aligned} \sum_{k'} \{H_{kk'} - EN_{kk'}\} f_{k'} &= 0, \quad H_{kk'} = \langle \phi_k | \hat{H} \hat{P}_{KK'}^I | \phi_{k'} \rangle, \\ N_{kk'}^I &= \langle \phi_k | \hat{P}_{KK'}^I | \phi_{k'} \rangle. \end{aligned} \quad (3)$$

It is clear that, using Eqs. (3), the eigenvalues  $E$  of  $H_{kk'}$  and the corresponding wave functions can be efficiently calculated. Two separable (pairing + quadrupole) interactions are included in the following PSM Hamiltonian:

$$\hat{H} = \hat{H}_0 - \frac{1}{2}\chi \sum_{\mu} \hat{Q}_{\mu}^{\dagger} \hat{Q}_{\mu} - G_M \hat{P}^{\dagger} \hat{P} - G_Q \sum_{\mu} \hat{P}_{\mu}^{\dagger} \hat{P}_{\mu}. \quad (4)$$

The first term is a Hamiltonian of the single particle deformed, and  $\chi$  is the strength of the quadrupole-quadrupole force; it is a function of the deformed constant  $\varepsilon$ . The strength  $\chi$  can be obtained self-consistently from the potentials of the Hartree-Nilsson model [33].  $G_M$  and  $G_Q$  are the monopole and quadrupole pairing strengths that represent a residual interaction in the BCS form. The residual interactions of monopole and quadrupole pairing act only in the nucleon valence space in the same major shell located near the Fermi surface [34]. The monopole interactions contribute to the energy gap  $\Delta$ . However, the quadrupole force can reproduce most efficiently of the crossing between neutron and proton bands [35]. It has been constituted that the strength pairing force for neutron and proton are associated with a model space. The monopole pairing strength can be defined in terms of the parameters  $G_1$  and  $G_2$  for the neutron and proton, respectively [36,37]:

$$G_M = \frac{G_1 \mp G_2 \frac{N-Z}{A}}{A}, \quad (5)$$

where the sign  $- (+)$  is for the neutron (proton), with  $G_1 = 19.86$ ,  $G_2 = 17.98$  taken from Ref. [38]. Due to the sensitivity of the MOI to the nuclear monopole pairing [39], we found it appropriate to renormalize the  $G_1$  parameter by a factor of 0.9176 for the  $^{242-246}\text{Pu}$  isotopes. The quadrupole pairing strength  $G_Q$  is assumed to be proportional to  $G_M$ .

In the PSM, the electric quadrupole transition probabilities  $B(E2)$  from the state  $|\psi^I\rangle$  to the state  $|\psi^{I-2}\rangle$  can be computed

TABLE I. Values of deformation parameters used in the model calculation.

|              | <sup>236</sup> Pu | <sup>238</sup> Pu | <sup>240</sup> Pu | <sup>242</sup> Pu | <sup>244</sup> Pu | <sup>246</sup> Pu |
|--------------|-------------------|-------------------|-------------------|-------------------|-------------------|-------------------|
| $\epsilon_2$ | 0.2510            | 0.2710            | 0.2502            | 0.2625            | 0.2678            | 0.2698            |
| $\epsilon_4$ | -0.0520           | -0.0570           | -0.0670           | -0.0440           | -0.0193           | -0.0034           |

as follows:

$$B(E2, I \rightarrow I - 2) = \frac{1}{2I + 1} |\langle \psi^{I-2} || \hat{Q}_2 || \psi^I \rangle|^2, \quad (6)$$

where  $\psi^{I-2}$  and  $\psi^I$  are the wave functions of a PSM system [Eq. (1)] for final and initial states, respectively. The effective charges used to calculate the  $B(E2)$  within the PSM are taken to be  $e^\pi = 1.5e$  and  $e^\nu = 0.5e$ . The magnetic properties of the yrast states are identified by measuring the effective gyromagnetic factor ( $g$  factor) of angular momentum ( $I$ ) using the following equations of the PSM [11]:

$$g(I) = \frac{\mu(I)}{\mu_N I} = \frac{1}{\mu_N I} [\mu_\pi(I) + \mu_\nu(I)] \quad (7)$$

and

$$\begin{aligned} \mu_\tau(I) &= \langle \psi^I | \hat{\mu}_z^\tau | \psi^I \rangle = \frac{I}{\sqrt{I(I+1)}} \langle \psi^I | \hat{\mu}^\tau || \psi^I \rangle \\ &= \frac{I}{\sqrt{I(I+1)}} [g_l^\tau \langle \psi^I | \hat{j}^\tau || \psi^I \rangle + (g_s^\tau - g_l^\tau) \langle \psi^I | \hat{s}^\tau || \psi^I \rangle], \end{aligned} \quad (8)$$

where  $\tau = \pi$  or  $\nu$ , and  $\mu_\pi(I)$  and  $\mu_\nu(I)$  are the proton and neutron magnetic moments of a state  $|\psi^I\rangle$  which are given in nuclear magneton units. The  $g_l$  and  $g_s$  are the standard values:  $g_l^\pi = 1$ ,  $g_l^\nu = 0$ ,  $g_s^\pi = 5.586 \times 0.75$ , and  $g_s^\nu = -3.826 \times 0.75$ . They are damped by a usual 0.75 factor from the free-nucleon values in order account for the core-polarization and meson-exchange current corrections [40].

### III. RESULTS AND DISCUSSION

The heavy nuclei at the gate to superheavy elements have large deformation with the axial deformation parameters. The adjustable parameters of the PSM Hamiltonian ( $\epsilon_2, \epsilon_4$ ) and pairing strengths of actinide nuclei involve several considerations. These are essentially selected to reproduce the observed kinematic  $j^{(1)}$  and dynamic  $j^{(2)}$  MOI, which represent the most crucial quantities characteristic of the superdeformed band. The deformation parameters (Table I) are determined within a reasonable range in the actinide mass region and do not deviate from the previous studies [26,41,42]. When tested against a wide range of parameters, they are found to confirm the results reported in literature. The PSM results of low-lying energy states of yrast bands for Pu nuclei are then compared with the experimental data [43]. Figure 1 illustrates this comparison and gives sufficient evidence of the success of the model parameters to reproduce the observation. To understand the yrast band and its wave functions in Pu nuclei, a theoretical treatment of the band diagram has been submitted in which the projected energies of 2qp nucleon bands appear [35].

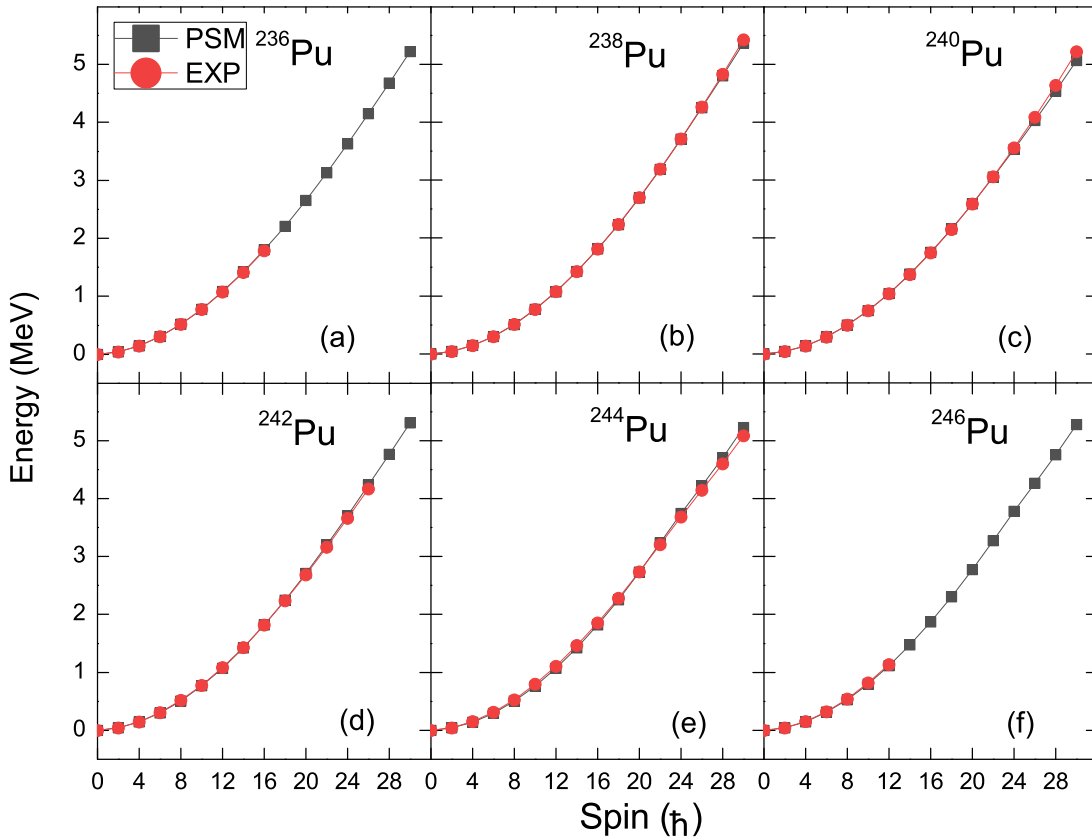


FIG. 1. A comparison between calculated positive-parity energy levels of yrast bands for <sup>236-246</sup>Pu and available experimental data [43].

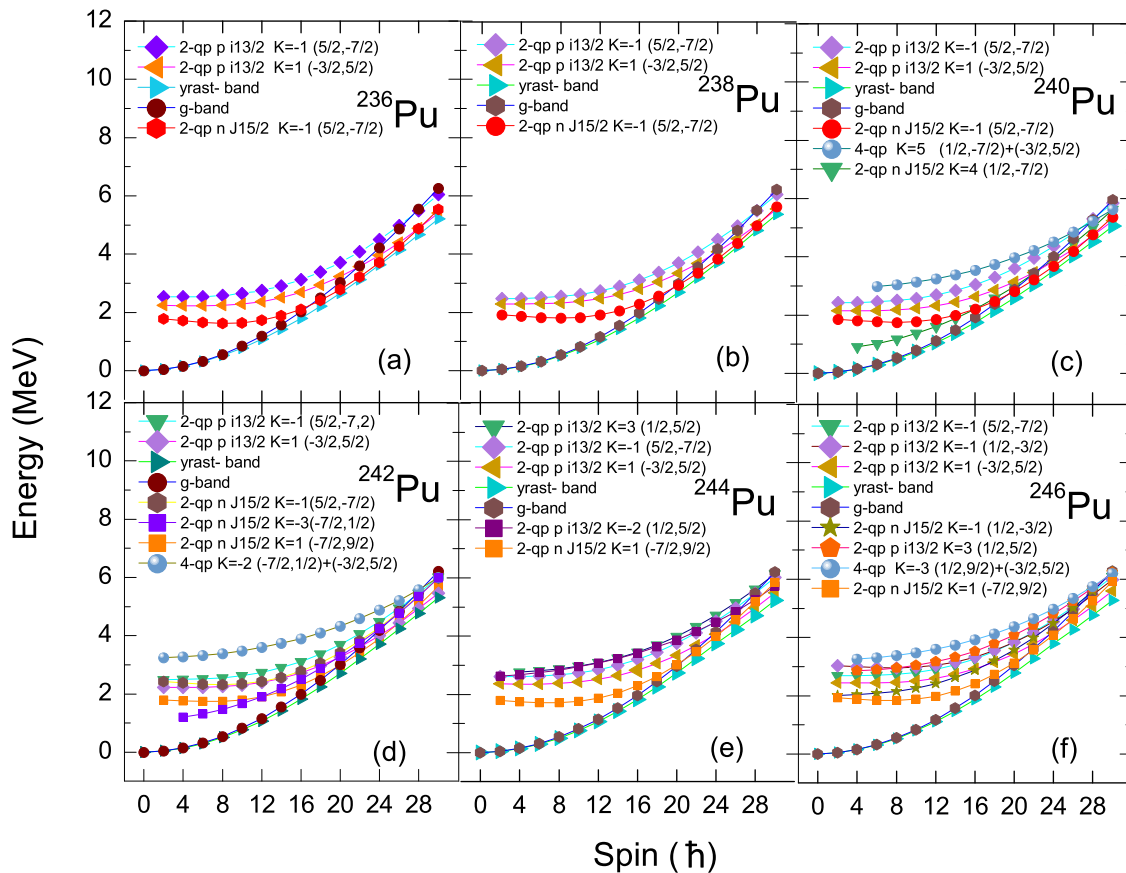


FIG. 2. Band diagrams for the low-lying states of  $^{236-246}\text{Pu}$ . Only the important configurations have been submitted: [(a) and (b)] Three 2qp bands, (c) four 2qp bands, [(d) and (e)] five 2qp bands, and (f) six 2qp bands.

The band diagrams for  $^{236-246}\text{Pu}$  shown in Fig. 2 include only important bands that have direct contributions to the yrast band. Also, the band diagram makes additional predictions regarding the crossing bands, backbending, upbending, and nucleon alignments. In the actinide, the intruder orbits are  $\nu(j_{15/2})$  for neutrons and  $\pi(i_{13/2})$  for protons [44]. In low-spin states, the yrast bands of the plutonium isotopes are constructed from a g band which has a vacuum with zero projection and configuration. But at high spins, the excited 2qp bands of  $\nu(j_{15/2})$  and  $\pi(i_{13/2})$  orbits are dominant. The interactions (crossings) between the s bands (superbands) and g bands in very heavy nuclei [45] result from the neutron alignment in high intruder orbits.

As to Fig. 2, it is observed that a relatively constant number of crossing points along the g band are occurring at certain values of spin. The lack of data in  $^{236}\text{Pu}$  and  $^{246}\text{Pu}$  isotopes prevents us from performing a thorough analysis of the structural changes in high spins of the yrast band. The diagrams in Fig. 2 demonstrated the first crossing of the neutrons  $\nu^2[5/2, -7/2]$ ,  $K^\pi = 1^-$  bands for  $^{236-240}\text{Pu}$  isotopes, while for  $^{242-246}\text{Pu}$  isotopes, the first crossing of neutrons  $\nu^2[5/2, -7/2]$ ,  $K^\pi = 1^+$ , occurs at a certain angular momentum  $I = 18$  and  $20$  for  $^{236}\text{Pu}$  and  $^{236-240}\text{Pu}$ , respectively. Moreover, before the crossing, there is a relatively large gap separating the s band of neutrons and the next band of protons, 2qp, with  $K^\pi = 1^+$  being approximately 0.6 MeV in

all the present nuclei. As it is known, the 4qp band is mainly composed of two-quasiparticle neutrons and protons whose energy has to be close in energy to the Fermi level [46]. Except for the  $K^\pi = 1^+$  neutron band, most reliable neutron single particles of  $^{236}\text{Pu}$  and  $^{238}\text{Pu}$  are far from the Fermi level, and consequently could not be given an assignment to construct the yrast band. Therefore, the 4qp bands are more energetic than g bands in these light isotopes. As to the  $^{240}\text{Pu}$  isotope, the 2qp neutron band emerges along with the configuration  $\nu^2[1/2, -7/2]$ ,  $K^\pi = 4^+$ , where these two neutrons have single-particle energies in the vicinity of the Fermi level. Interestingly, the  $K^\pi = 4^+$  neutron pair has been observed to be competition with the proton pair of the  $\pi^2[-3/2, 5/2]$ ,  $K^\pi = 1^+$ , band in order to cross the g band at  $I = 22$  [47]. As seen from Fig. 2(c) the 4qp band which is composed of  $\nu^2[1/2, -7/2]$ ,  $K^\pi = 4^+$ , and  $\pi^2[-3/2, 5/2]$ ,  $K^\pi = 1^+$ , crosses the g band after competing with the  $\pi^2[5/2, -7/2]$ ,  $K^\pi = 1^-$ , proton band at  $I = 28$ . Another neutron alignment can be seen in the  $^{242}\text{Pu}$  band diagram;  $\nu^2[-7/2, 1/2]$ ,  $K^\pi = 3^-$ , and  $\nu^2[5/2, -7/2]$ ,  $K^\pi = 1^-$  cross the g band at  $I = 24$  and  $26$ , respectively. They seem to appear pairwise, with an almost degenerated energy in high-spin states. For  $^{242}\text{Pu}$  the crossing between the 4qp band and the g band is seen at  $I = 28$ . Numerous 2qp proton bands have been obtained for  $^{244}\text{Pu}$  and  $^{246}\text{Pu}$  isotopes while their neutron counterparts are absent in  $^{244}\text{Pu}$  [see Figs. 2(e) and 2(f)]. There is a striking

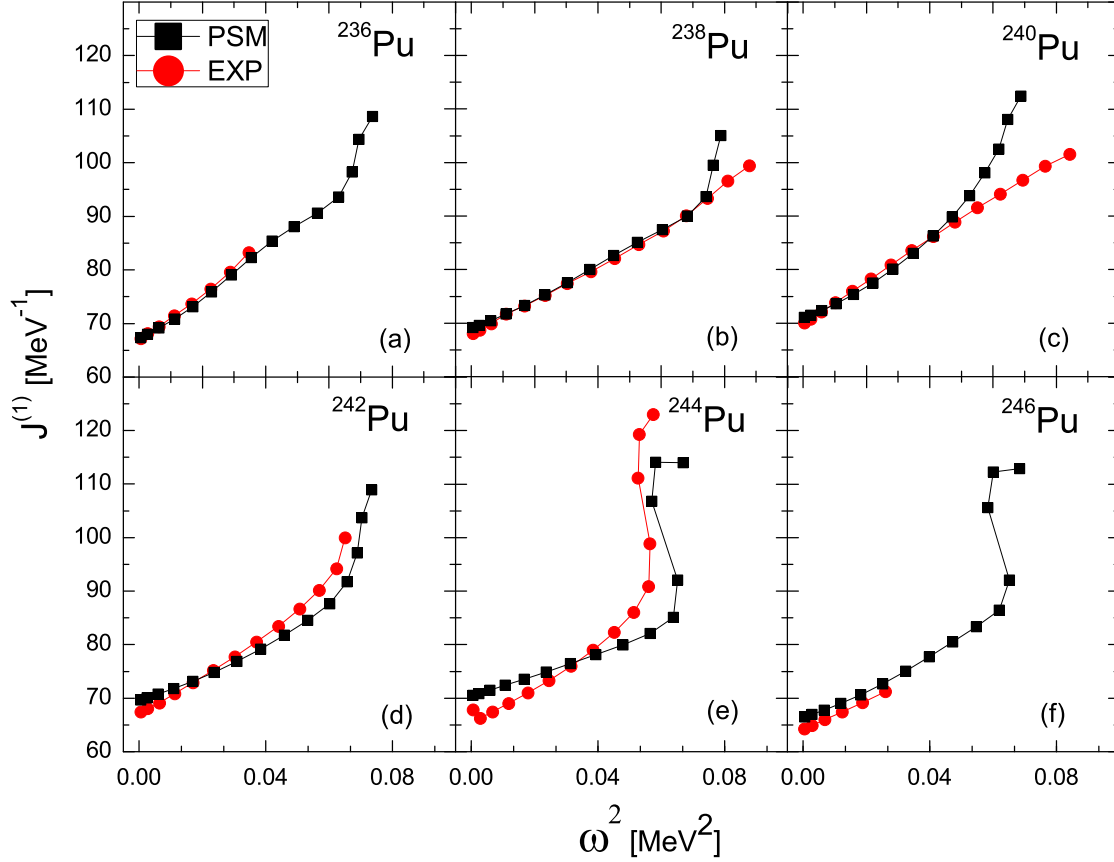


FIG. 3. Kinematic moment of inertia  $j^{(1)}$  for  $^{236-246}\text{Pu}$  calculated by the PSM as a function of the rotational frequency  $\omega^2$ , in comparison with experimental [43], experimental (circle), and theoretical (square) values.

competition between  $\nu^2[1/2, -3/2]$ ,  $K^\pi = 1^-$ ,  $\pi^2[1/2, -3/2]$ ,  $K^\pi = 1^-$ , and  $\pi^2[5/2, -7/2]$ ,  $K^\pi = 1^-$  bands to cross the g band at around  $I = 28$ . The similarity in their  $K^\pi$  values is worth noting. We can also see in Fig. 2(f) another competition between the 4qp band and  $\pi^2[1/2, 5/2]$ ,  $K^\pi = 3^+$  band to cross the g band at  $I = 30$ .

The selected parameters for deformation and pairing force describe precisely the rotational properties of the collective prolate shape. Generally, there are important features that can be described in terms of MOI [48]. The energy spacing between any two successive spins is devoted to calculating the moments of inertia of the yrast band. The  $j^{(1)}$  and  $j^{(2)}$  for the yrast band energy levels were obtained by using the following equations [11,49]:

$$j^{(1)} = \frac{2I - 1}{E(I) - E(I - 2)}, \quad (9)$$

$$j^{(2)} = \frac{4}{(E(I) - E(I - 2)) - (E(I - 2) - E(I - 4))}, \quad (10)$$

and the rotational frequency is given by

$$\omega = \frac{E(I) - E(I - 2)}{2}. \quad (11)$$

The dependence of the MOI on the rotational frequencies  $\omega$  is shown in Fig. 3. More precisely, two important effects can

be recognized along the yrast line of  $^{242-246}\text{Pu}$  isotopes: First, the pairing correlations between nucleons at low spins, and second, the Coriolis antipairing (CAP) [50–52] and rotation alignment (RAL) at high spins [46,53]. The Coriolis force is going to be prohibitively complex at high spins because of the band crossings in this region as indicated earlier. As shown in Figs. 3(a) and 3(b) the calculated  $j^{(1)}$  values of yrast bands are compared with the available data. From the calculations, we note that  $j^{(1)}$  in  $^{236}\text{Pu}$ ,  $^{238}\text{Pu}$ , and  $^{240}\text{Pu}$  increased gently with  $\omega^2$  up to  $I = 24$ , 26, and 20, respectively. The critical frequencies ( $\omega_c$ ) of these nuclei are 0.251, 0.272, and 0.219 MeV. The PSM predicts an upbend which occurs in high-spin states in  $^{236-240}\text{Pu}$  isotopes. The appearance of upbending in the three lightest Pu isotopes was not predicted by experimental data.

The full experimental data of  $j^{(1)}$  for  $^{238}\text{Pu}$  and  $^{240}\text{Pu}$  indicate that the linearity of  $j^{(1)}$  versus  $\omega^2$  remains unchanged. The linearity could occur due to the strong octupole correlation between two quasiparticles near the Fermi surface that affect the wave functions of the low- and high-spin yrast band of both isotopes [24,25] [see Figs. 3(b) and 3(c)]. So the band diagram of  $^{238,240}\text{Pu}$  includes different excitation energy bands: Two of them are the  $\pi^2[5/2, -7/2]$ ,  $K^\pi = 1^-$  proton alignment of  $^{238}\text{Pu}$  and  $\nu^2[1/2, -7/2]$ ,  $K^\pi = 4^+$  neutron alignment of  $^{240}\text{Pu}$ , which cross the g band at  $I = 28$  and 22, respectively. For  $^{240}\text{Pu}$ , it should be noted that



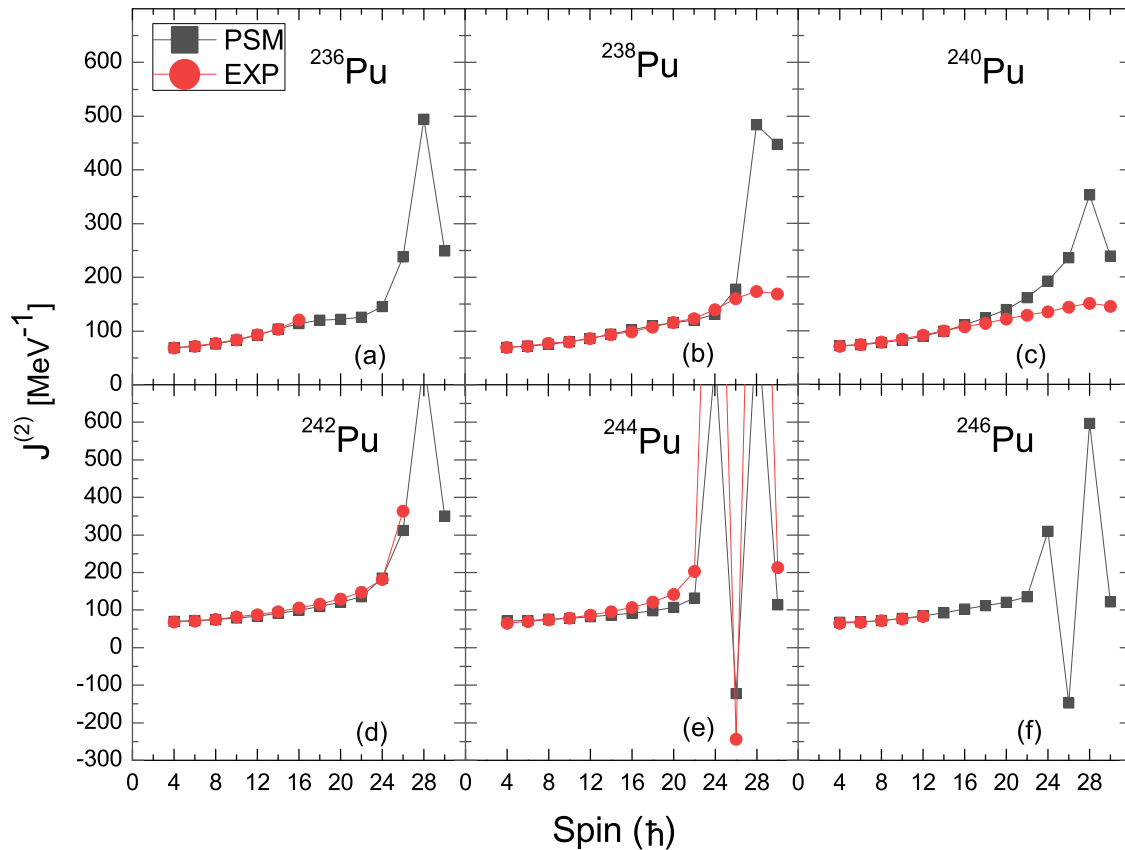


FIG. 4. Dynamic moment of inertia  $j^{(2)}$  as a function of spin for  $^{236-246}\text{Pu}$ .

the simultaneous crossing of the neutron  $\nu^2[1/2, -7/2]$ ,  $K^\pi = 4^+$  and proton  $\pi^2[-3/2, 5/2]$ ,  $K^\pi = 1^+$  bands at  $I = 22$  [shown in Fig. 2(c)] represents equal excitation energies of two neutrons and two protons at a certain angular momentum. Moreover, according to PSM results, the two interesting neutrons  $[1/2, -7/2]$  and protons  $[-3/2, 5/2]$  from  $j_{15/2}$  and  $i_{13/2}$  are pretty close to the Fermi level and align fast [4]. Thus, the yrast band will be built from these bands as well as from the neutron  $\nu^2[5/2, -7/2]$ ,  $K^\pi = 1^-$  band more than other bands as clear in diagram in Fig. 2(c). Because of it, we can attribute the deviation between the theory and the data curve in Fig. 3(c) after  $I = 22$  to the crossing of the  $K^\pi = 4^+$  and  $K^\pi = 1^+$  bands. Figure 3(d) shows a remarkable conformity between the calculated and experimental data in the tendency of the  $j^{(1)}$  against  $\omega^2$ . The PSM results for  $^{242}\text{Pu}$  show an upbending in  $j^{(1)}$  at a high spin due to the crossings of multiquasineutron bands with the g band. The critical frequency which corresponds to the upbending in  $^{242}\text{Pu}$  is equal to  $\omega_c = 0.256$  MeV. The prediction of the upbending in  $^{242}\text{Pu}$  agrees reasonably with the observations in Ref. [54].

For the  $^{244}\text{Pu}$  isotope, as seen in Fig. 3(e) the calculated  $j^{(1)}$  before the first crossing of two quasineutrons with  $\nu^2[-7/2, 9/2]$ ,  $K^\pi = 1^+$  at  $I = 20$  increases gently in a rotational frequency. After  $I = 20$ , the consequences of protons domination become more pronounced and they contribute to the irregularity in the yrast state energies. The upbendings in the  $^{244}\text{Pu}$  occur at  $I = 22$  and  $\omega_c = 0.237$  MeV. Similarly,

the experimental upbendings of  $^{244}\text{Pu}$  occur at  $I = 22$  and  $\omega_c = 0.226$  MeV. The theoretical  $j^{(1)}$  curve of  $^{244}\text{Pu}$  refers to the existence of one backbending at  $I = 24$  and  $\omega_c = 0.255$  MeV. Furthermore, there is a backbending in the experimental  $j^{(1)}$  curve at  $I = 24$  and  $\omega_c = 0.237$  MeV which is reproduced accurately by PSM calculations [54].

We expect that the significant dominance of aligned protons which occupied their excited bands in  $^{244}\text{Pu}$  has led to backbending compared to other isotopes [55]. Theoretically, there is a plateau occurring at the interval of spin  $I = 28-30$ , and the energies do not depend on spin (basically, the MOI is spin independent within a certain range in this region) [56]. According to PSM results, the plateau is simultaneously formed when two successive crossing points are formed by two parallel excited bands of  $\pi^2[5/2, -7/2]$ ,  $K^\pi = 1^-$  and  $\pi^2[1/2, 5/2]$ ,  $K^\pi = 3^+$ , respectively. To date, the available experimental data about  $^{246}\text{Pu}$  do not cover most of the interesting high-spin region. Similar to  $^{244}\text{Pu}$ , the upbending, backbending, and plateau are observed in the  $j^{(1)}$  curve of the heavier isotope  $^{246}\text{Pu}$ . The investigations on the  $j^{(1)}$  behavior demonstrate that there is no backbending in  $^{236}\text{Pu}$ ,  $^{238}\text{Pu}$ ,  $^{240}\text{Pu}$ , and  $^{242}\text{Pu}$ , while it is present in  $^{244}\text{Pu}$  and  $^{246}\text{Pu}$  because of the simultaneous breaking of the  $i_{13/2}$  abundant proton pairs.

Figure 4 shows the experimental and calculated values of  $j^{(2)}$  of Pu isotopes. One can see that the PSM predictions reasonably reproduce the current data tendency, whereby the  $j^{(2)}$

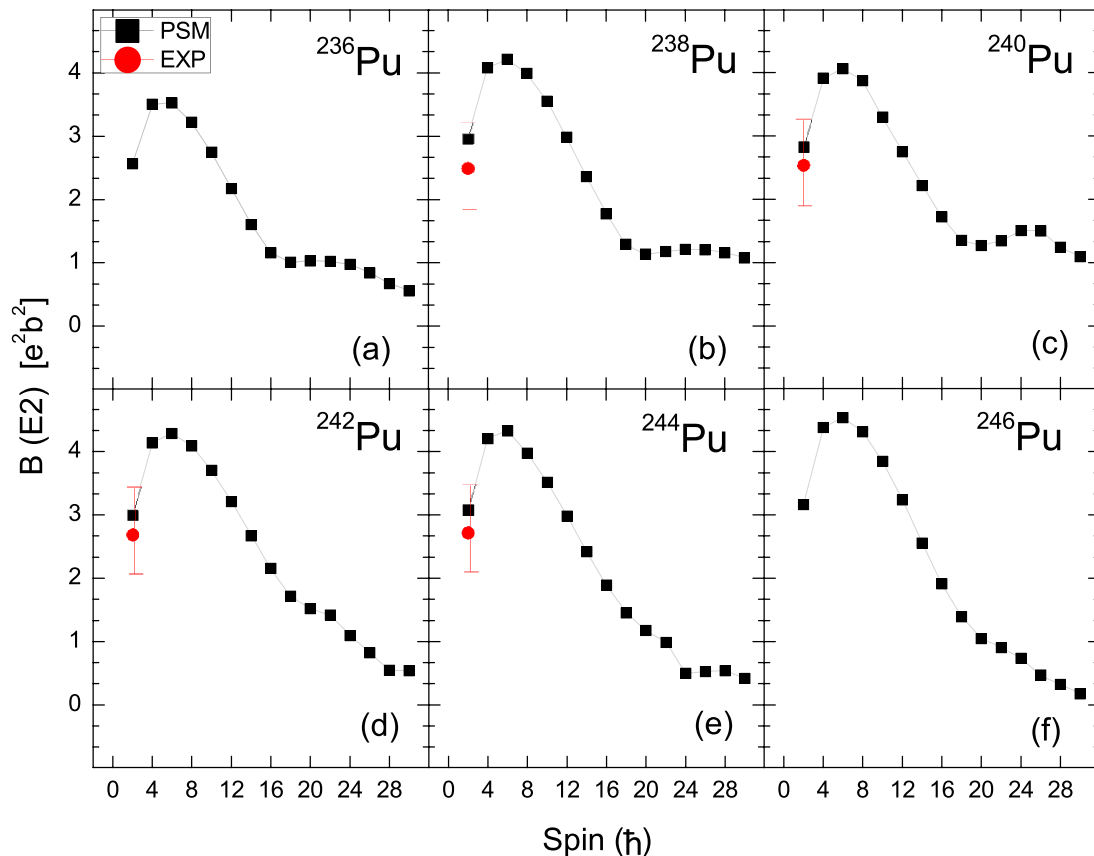


FIG. 5. Available experimental and calculated  $B(E2; I \rightarrow I - 2)$  values (in  $e^2 b^2$ ) for  $^{236-246}\text{Pu}$  isotopes.

value is extremely sensitive to any difference in pairing and deformation parameters [57–59]. In this respect, our choice of the values of PSM parameters (Table I) was extremely thorough. For  $^{236-240}\text{Pu}$  isotopes, the calculated dynamic moments of inertia  $j^{(2)}$  are shown in Figs. 4(a)–4(c). One upturning of  $j^{(2)}$  at  $I = 28$  has been predicted. In the heavier isotopes  $^{242-246}\text{Pu}$ , it is essential to remark that the theory and the available experimental data of the  $j^{(2)}$  predicted an anomaly in the high-spin states. Together, they also refer to the presence of downturns followed by an upturn. The obtained results for  $^{242}\text{Pu}$  [Fig. 4(d)] reproduced very well the observed  $j^{(2)}$ , which predicts one upturning at  $I = 28$ . For the  $^{244}\text{Pu}$  isotope, there are two upturnings at  $I = 24$  and  $28$  and one downturning at  $I = 26$  of the striking anomaly in the  $j^{(2)}$  values and their positions are well reproduced. Accordingly, a good agreement has been achieved between PSM calculations and experimental data of  $j^{(2)}$ . The existence of an anomaly has also been predicted in  $^{246}\text{Pu}$  as in the  $^{244}\text{Pu}$  isotope.

The  $E2$  transition probabilities have been calculated using Eq. (6). Experimentally, the  $B(E2; 2_1^+ \rightarrow 0_1^+)$  values of  $^{238-244}\text{Pu}$  are the only ones available, as shown in Fig. 5. According to PSM results, there was a noticeable rise in  $B(E2)$  from spin  $I = 2$  to  $6$ . Each isotope's  $B(E2)$  value peaked at spin  $I = 6$  and then fell all the way to spin  $I = 18$ . The change in the structure of the yrast band caused by the crossing of the  $g$  band by the  $2qp$  bands may have caused the decrease in  $B(E2)$  values. In the case of  $^{236,238}\text{Pu}$  isotopes, according to

the calculated values, a slight deviation in the transition probability values appears with the increase in the spin ( $I = 18-30$ ). With the increase in the effect of the neutron bands, the behavior of the  $B(E2)$  values begins to change with an increase in spin as in the  $^{240}\text{Pu}$  isotopes. There is a relatively small peak in the  $B(E2)$  curve, which is attributed to the rotational alignment of neutrons in  $i_{15/2}$  with  $\nu^2[1/2, -7/2]$ ,  $K^\pi = 4^+$  configuration and protons in  $i_{13/2}$  with  $\pi^2[-3/2, 5/2]$ ,  $K^\pi = 1^+$  configuration which are in competition to cross the  $g$ -band (see Fig. 2). For  $^{242}\text{Pu}$ , one can note a dip in  $B(E2)$  values at  $I = 22$  up to  $28$  followed by linear behavior. But in the case of  $^{244}\text{Pu}$ , the dip in  $B(E2)$  occurs only between  $I = 22$  and  $24$ . Finally for  $^{246}\text{Pu}$ , only a dip in  $B(E2)$  values can be observed at  $I = 22$ . We attribute variations in  $B(E2)$  behavior along high-spin states to the different contributions of the aligning protons and neutrons in their intruder orbits and subsequently to the sharp changes in the wave functions.

The  $g$  factor of spin  $I$  is very sensitive to the nucleon alignment in its high- $j$  intruder orbits, calculated directly by many-body wave functions of the PSM. The  $g$  factors of Pu isotopes against spin  $I$  are displayed in Fig. 6. For each nucleus, the trend of the  $g$  factor with the spin remains almost constant up to the points where the first crossings occur because at low spins the dominant contribution of the yrast band is the  $K = 0$  band ( $g$  band). However, an increase in  $g$ -factor values at  $I > 20$  is predicted with an upbending at high spins. The occurrence of upbendings in  $^{236,240}\text{Pu}$  and  $^{242-246}\text{Pu}$

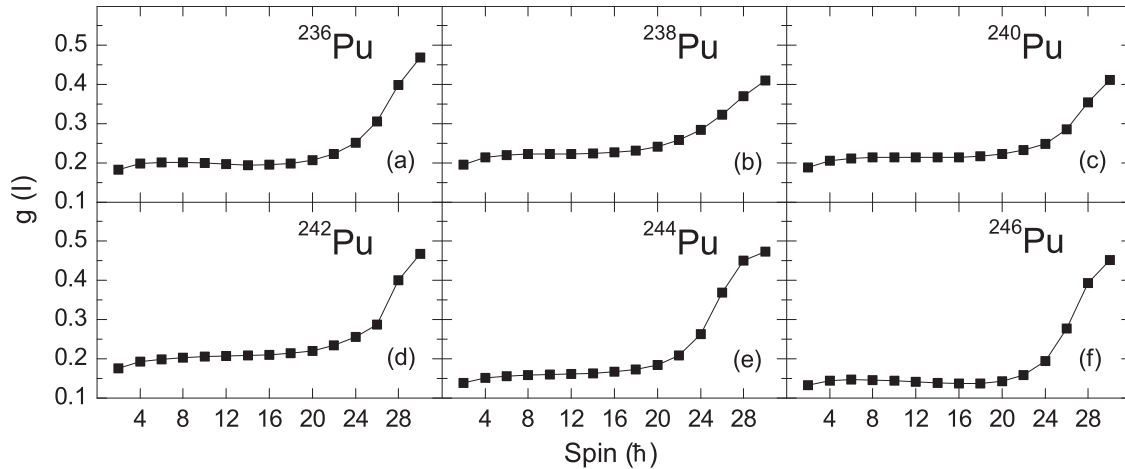


FIG. 6.  $g$ -factor values predicted by PSM calculations for (a)  $^{236}\text{Pu}$ , (b)  $^{238}\text{Pu}$ , (c)  $^{240}\text{Pu}$ , (d)  $^{242}\text{Pu}$ , (e)  $^{244}\text{Pu}$ , and (f)  $^{246}\text{Pu}$ . All are clearly similar in spin dependence.

isotopes are due to the alignment of proton  $\pi^2[5/2, -7/2]$ ,  $K^\pi = 1^-$  and  $\pi^2[-3/2, 5/2]$ ,  $K^\pi = 1^+$  bands which are larger in heavier isotopes. However, this characteristic of the isotopes is still experimentally unknown.

#### IV. CONCLUSION

We conducted a study of energy levels of yrast bands for several Pu isotopes. The band diagram of the present nuclei has been investigated, including multirotational bands of excited quasiparticles; the rotational bands that have not been involved in the building of yrast bands are not shown. The intruder orbits of the actinide nuclei are  $j_{15/2}$  for neutrons and  $i_{13/2}$  for protons which would strongly contribute to the angular momentum alignment in this mass region. The behavior of 2qp bands was explored in the diagram of the bands. Depending on the band diagram, we predict that the first crossings between s bands and g bands occur at  $I = 18$  in  $^{236}\text{Pu}$  and at  $I = 20$  in  $^{238-246}\text{Pu}$  which are caused by the alignment of two quasineutrons in the excited bands of the  $j_{15/2}$  orbit. We also found that the contributions of two quasiprotons to the construction of the yrast band were small in  $^{236-240}\text{Pu}$ , but big in the heavier isotopes. A competition between the  $\nu(j_{15/2})$  and  $\pi(i_{13/2})$  alignment at spin  $I = 22$  has been suggested in the case of the  $^{240}\text{Pu}$  isotope. The deviation between the theory and data, which can be seen in Figs. 3(c) and 4(c) of  $^{240}\text{Pu}$ , is due to the alignment of the neutrons in the  $\nu^2[1/2, -7/2]$ ,  $K^\pi = 4^+$  band which crosses g band at  $I = 22$ . The aligning pro-

cesses of  $\pi^2(i_{13/2})$  appear more frequently in the  $^{244,246}\text{Pu}$  than  $^{236-242}\text{Pu}$  isotopes; therefore, we predict a backbending in the  $j^{(1)}$  plot of the  $^{244,246}\text{Pu}$  as an outcome of these processes. The observed backbending is reproduced well by our PSM results. A plateau in  $j^{(1)}$  was seen in the  $I = 28-30$  region of  $^{244,246}\text{Pu}$ . The anomaly in  $j^{(2)}$  is observed at high spins and corresponds to the crossing points between different quasiparticle bands that form the yrast band.

We observe pronounced peaks in  $j^{(2)}$  experimental data at a spin  $I = 28$  which are reproduced by our calculations. In the heavier  $^{242-246}\text{Pu}$  isotopes, both the theory and the known experimental data of  $j^{(2)}$  predict an anomaly in the high-spin-states region. The calculations  $j^{(2)}$  obtained for  $^{242}\text{Pu}$  reproduced perfectly the observed  $j^{(2)}$  moment. For  $^{244}\text{Pu}$ , the agreement with observational data is seemingly good. For all nuclei, we detected a pronounced increase in  $B(E2)$  at lower spins. Many dips and flattenings at high-spin regions attributed to the different contributions of multi-quasiparticle configurations were predicted. The behavior of  $g$  factors along with the spin for all present isotopes is almost the same up to around  $I = 18$ . An increase in  $g$  factors is observed only at high spins where crossings of bands occur. Due to the rarity of available experimental information, the PSM predictions will be helpful for future experiments.

#### ACKNOWLEDGMENTS

The authors would like to thank Prof. Y. Sun for his interest in the subject and his many helpful suggestions.

- [1] Y. Zhao and A. Arima, *Phys. Rep.* **545**, 1 (2014).  
 [2] T. Kouno, C. Ishizuka, T. Inakura, and S. Chiba, *Prog. Theor. Exp. Phys.* **2022**, 023D02 (2022).  
 [3] J. Dukelsky, S. Lerma H., L. M. Robledo, R. Rodriguez-Guzman, and S. M. A. Rombouts, *Phys. Rev. C* **84**, 061301(R) (2011).  
 [4] R. Bengtsson, *Journal De Physique* **41**, C10-84 (1980).

- [5] Y. Sun, *Phys. Scr.* **91**, 043005 (2016).  
 [6] D. V. Shirkov, *Phys. Usp.* **52**, 549 (2009).  
 [7] T. Ya, Y. J. Chen, Y. S. Chen, Z. C. Gao, and L. Liu, *Phys. Rev. C* **104**, 014306 (2021).  
 [8] R. S. Simon, F. Folkmann, GSI Darmstadt, J. Libert, J. P. Thibaud, R. J. Walen, and S. Frauendorf, *Z. Phys. A: At. Nucl.* **298**, 121 (1980).



- [9] G. Hackman, R. V. F. Janssens, T. L. Khoo, I. Ahmad, J. P. Greene, H. Amro, D. Ackermann, M. P. Carpenter, S. M. Fischer, T. Lauritsen, L. R. Morss, P. Reiter, D. Seweryniak, D. Cline, C. Y. Wu, E. F. Moore, and T. Nakatsukasa, *Phys. Rev. C* **57**, R1056 (1998).
- [10] A. V. Afanasjev, *Phys. Scr.* **89**, 054001 (2014).
- [11] K. Hara and Y. Sun, *Int. J. Mod. Phys. E* **04**, 637 (1995).
- [12] L. J. Wang, Y. Sun, T. Mizusaki, M. Oi, and S. K. Ghorui, *Phys. Rev. C* **93**, 034322 (2016).
- [13] P. Kumar and S. K. Dhiman, *Mod. Phys. Lett. A* **35**, 2050189 (2020).
- [14] S. Singh, S. Guptab, A. Guptab, A. Kumar, A. Bharti, G. H. Bhat, and J. A. Sheikh, *Chin. J. Phys.* **62**, 240 (2019).
- [15] J. A. Sheikh and K. Hara, *Phys. Rev. Lett.* **82**, 3968 (1999).
- [16] S. Jehangir, G. H. Bhat, J. A. Sheikh, R. Palit, and P. A. Ganai, *Nucl. Phys. A* **968**, 48 (2017).
- [17] S. Jehangir, G. H. Bhat, J. A. Sheikh, S. Frauendorf, W. Li, R. Palit, and N. Rather, *Eur. Phys. J. A* **57**, 308 (2021).
- [18] M. Rajput, S. Singh, P. Verma, V. Rani, A. Bharti, G. H. Bhat, and J. A. Sheikh, *Nucl. Phys. A* **1019**, 122383 (2022).
- [19] S. Jehangir, N. Nazir, G. H. Bhat, J. A. Sheikh, N. Rather, S. Chakraborty, and R. Palit, *Phys. Rev. C* **105**, 054310 (2022).
- [20] J. W. Cui, X. R. Zhou, F. Q. Chen, Y. Sun, C. L. Wu, and Z. C. Gao, *Phys. Rev. C* **90**, 014321 (2014).
- [21] R. S. Guo, L. M. Chen, and C. H. Chou, *J. Phys. G: Nucl. Part. Phys.* **32**, 269 (2006).
- [22] F. Al-Khudair, G. L. Long, and Y. Sun, *Phys. Rev. C* **79**, 034320 (2009).
- [23] Z. Zhou, Y. Liu, Y. Yang, F. Chen, and Y. Sun, *Chin. Sci. Bull.* **59**, 3853 (2014).
- [24] I. Wiedenhöver, R. V. F. Janssens, G. Hackman, I. Ahmad, J. P. Greene, H. Amro, P. K. Bhattacharyya, M. P. Carpenter, P. Chowdhury, J. Cizewski, D. Cline, T. L. Khoo, T. Lauritsen, C. J. Lister, A. O. Macchiavelli, D. T. Nisius, P. Reiter, E. H. Seabury, D. Seweryniak, S. Siem *et al.*, *Phys. Rev. Lett.* **83**, 2143 (1999).
- [25] X. T. He and Y. C. Li, *Phys. Rev. C* **102**, 064328 (2020).
- [26] S. G. Nilsson, C. Fu Tsang, A. Sobiczewski, Z. Szymański, S. Wycech, C. Gustafson, I. L. Lamm, P. Möller, and B. Nilsson, *Nucl. Phys. A* **131**, 1 (1969).
- [27] Y. Sun, J. Y. Zhang, and M. Guidry, *Phys. Rev. Lett.* **78**, 2321 (1997).
- [28] A. Bohr, *Phys. Rev.* **81**, 134 (1951).
- [29] A. Bohr and B. Mottelson, *Mat. Fys. Medd. Dan. Vid. Selsk.* **27**, 1 (1957).
- [30] P. Ring and P. Schuck, *The Nuclear Many-Body Problem* (Springer, Berlin, 1980).
- [31] K. Hara and S. Iwasaki, *Nucl. Phys. A* **332**, 61 (1979).
- [32] K. Hara and Y. Sun, *Nucl. Phys. A* **529**, 445 (1991).
- [33] V. Velázquez, J. G. Hirsch, and Y. Sun, *Nucl. Phys. A* **643**, 39 (1998).
- [34] Z. Szymański, *Nucl. Phys.* **28**, 63 (1961).
- [35] S. Iwasaki and K. Hara, *Prog. Theor. Phys.* **68**, 1782 (1982).
- [36] I. L. Lamm, *Nucl. Phys. A* **125**, 504 (1969).
- [37] K. Hara and S. Iwasaki, *Nucl. Phys. A* **348**, 200 (1980).
- [38] Z. Patyk and A. Sobiczewski, *Nucl. Phys. A* **533**, 132 (1991).
- [39] Y. Sun and M. Guidry, *Phys. Rev. C* **52**, R2844 (1995).
- [40] S. Raman, C. W. Nestor, and P. Tikkanen, *At. Data Nucl. Data Tables* **78**, 1 (2001).
- [41] S. Ćwiok, S. Hofmann, and W. Nazarewicz, *Nucl. Phys. A* **573**, 356 (1994).
- [42] P. Möller, A. J. Sierk, T. Ichikawa, and H. Sagawa, *At. Data Nucl. Data Tables* **109-110**, 1 (2016).
- [43] ENSDF, Nuclear Data Sheet, <http://www.nndc.bnl.gov/ensdf>.
- [44] H. Ower, T. W. Elze, J. Idzko, and K. Stelzer, *Nucl. Phys. A* **388**, 421 (1982).
- [45] J. Egido and P. Ring, *Nucl. Phys. A* **423**, 93 (1984).
- [46] F. S. Stephens and R. S. Simon, *Nucl. Phys. A* **183**, 257 (1972).
- [47] M. Płoszajczak and A. Faessler, *J. Phys. G: Nucl. Phys.* **8**, 709 (1982).
- [48] F. S. Stephens, *Phys. Scr.* **1983**, 5 (1983).
- [49] C. K. Ross and Y. Nogami, *Nucl. Phys. A* **211**, 145 (1973).
- [50] B. Mottelson and J. Valatin, *Phys. Rev. Lett.* **5**, 511 (1960).
- [51] J. G. Valatin, in *Lectures in Theoretical Physics*, edited by W. E. Brittin, B. W. Downs, and J. Downs (Interscience, New York, 1962), Vol. 4.
- [52] A. Faessler, W. Greiner, and R. K. Sheline, *Nucl. Phys.* **62**, 241 (1965).
- [53] A. Faessler, K. R. Sandhya Devi, F. Grümmer, K. W. Schmid, and R. R. Hilton, *Nucl. Phys. A* **256**, 106 (1976).
- [54] W. Spreng, P. Azgui, H. Emling, E. Grosse, R. Kulesa, Ch. Michel, D. Schwalm, R. S. Simon, and H. J. Wollersheim, *Phys. Rev. Lett.* **51**, 1522 (1983).
- [55] M. J. A. de Voigt, J. Dudek, and Z. Szymański, *Rev. Mod. Phys.* **55**, 949 (1983).
- [56] Y. Sun and D. Feng, *Phys. Rep.* **264**, 375 (1996).
- [57] P. H. Heenen and R. V. F. Janssens, *Phys. Rev. C* **57**, 159 (1998).
- [58] A. Ibáñez-Sandoval, M. E. Ortiz, V. Velázquez, A. Galindo-Uribarri, P. O. Hess, and Y. Sun, *Phys. Rev. C* **83**, 034308 (2011).
- [59] C. S. Wu, L. Cheng, C. Z. Lin, and J. Y. Zeng, *Phys. Rev. C* **45**, 2507 (1992).